

Hybrid simulations of collapse of Alfvénic wave packets

B. Buti^{a)}

Jet Propulsion Laboratory, California Institute of Technology, Pasadena, California 91109

M. Velli

Dipartimento di Astronomia e S. dello Spazio, Largo E. Fermi 5, 50125 Firenze, Italy

P. C. Liewer and B. E. Goldstein

Jet Propulsion Laboratory, California Institute of Technology, Pasadena, California 91109

T. Hada

Interdisciplinary Graduate School of Engineering Sciences, Kyushu University, Fukuoka 816-8580, Japan

(Received 31 December 1999; accepted 29 June 2000)

Nonlinear dynamics, of large-amplitude circularly polarized Alfvénic wave packets, is investigated using a one-dimensional hybrid model. Kinetic effects such as finite-Larmor radius and nonlinear Landau damping, which become significant for plasmas with $\beta \sim 1$, are appropriately accounted for in these high-resolution hybrid simulations. Spatio-temporal evolution, of the left-hand polarized (LHP) wave packets, shows that they collapse because of the decreasing dispersive effects. However, singularities are arrested by the wave-particle interactions. At some critical time t_c , which depends on the plasma β and the initial amplitude of the wave packet, we observe a turning point. At this turning point, the polarization changes from LHP to RHP (right-hand polarized). The wave packet then starts broadening due to increasing dispersion associated with the RHP. Implications of collapse of the magnetic structures are briefly discussed. © 2000 American Institute of Physics. [S1070-664X(00)02810-X]

I. INTRODUCTION

Alfvén waves are a ubiquitous feature of magnetoplasmas. Implications of the existence of large-amplitude Alfvén waves in many cosmic plasmas have been investigated by a number of authors. Some of these examples include turbulent heating of solar corona,¹ coherent radio emissions,² interstellar scintillations of radio sources,³ generation of stellar winds and extragalactic jets, etc.⁴ Alfvén wave trains as well as Alfvénic turbulence have long been observed in space plasmas,^{5,6} e.g., solar wind, terrestrial magnetosphere, etc. In the cometary environment, some observations of solitary magnetic pulses have also been reported.⁷

To study the dynamical behavior of large-amplitude Alfvén waves, one can either use the full set of dispersive magnetohydrodynamic (MHD) equations and be satisfied with their numerical solutions or use an evolution equation derived from these MHD equations. The most popular evolution equation, governing nonlinear Alfvén waves, is the Derivative Nonlinear Schrödinger (DNLS) equation.⁸⁻¹¹ The big advantage of dealing with the DNLS is that it can be solved analytically.^{8,12,13} However, one should bear in mind that the DNLS is derived on the assumption that plasma β (the ratio of the kinetic pressure to the magnetic pressure) is not ~ 1 . Moreover it is valid for finite but not for very large ($\delta B/B \geq 1$) amplitude waves since terms higher than cubic nonlinearities are neglected in the derivation of the DNLS equation. For systems with $\beta \sim 1$, kinetic effects^{11,14-16} as well as coupling between magnetic field fluctuations and

density fluctuations^{17,18} become significant. To incorporate these effects in the studies of nonlinear dynamical Alfvén waves, one has to do dispersive magneto-hydrodynamic (MHD)^{19,20} and kinetic simulations. The Hall MHD simulations, done by Buti *et al.*¹⁹ and Velli *et al.*,²⁰ show that the Alfvén solitons get disrupted. Moreover, one observes the steepening of these waves with the emission of high-frequency radiations. On the other hand, the driven DNLS equation leads to chaos and turbulence in Alfvénic systems.²¹⁻²⁸ Inhomogeneities, in the magnetic field and the plasma densities, also destroy the coherent Alfvénic wave packets.²⁹

In the present paper, we have included the finite-Larmor radius effects, as well as the nonlinear wave particle interactions, for studying the spatio-temporal evolution of large-amplitude Alfvénic wave packets by means of hybrid simulations. These investigations have primarily been motivated by our recent high-resolution dispersive-MHD simulations which lead to blowing up of the left-hand polarized (LHP) Alfvénic wave packets (to be published). This blowup is due to an increase in the amplitude of the wave packet as it evolves. Our hybrid simulations clearly show the significant role of kinetic effects in inhibiting such blow ups. We see the amplitude increasing and at the same time the width of the packet decreases. This process of collapse continues until some critical time (t_c) that corresponds to the dynamical turning point. The term “dynamical turning point” is used simply to distinguish it from the usual turning point (also known as a reflection point). The reflection point is independent of time whereas the dynamical turning point appears due to dynamical evolution and has a functional dependence

^{a)}Electronic mail: bbuti@jplsp2.jpl.nasa.gov

on time. At time t_c dispersion takes over the nonlinearities and consequently the polarization flips from LHP to RHP (right-hand polarized). Further at the dynamical turning point, the scale size of the wave packet becomes small enough for the finite ion gyroradius effects to start playing an important role. The significant roles of kinetic effects as well as the coupling between density fluctuations and magnetic field fluctuations are quite evident from our simulations. To our knowledge, this is the first time that implications of the dynamical turning points, to the nonlinear evolution of the magnetic structures, are pointed out.

II. SIMULATION MODEL OF ALFVÉNIC WAVE PACKETS

Let us consider a two-species plasma, which is embedded in a uniform magnetic field \mathbf{B}_0 oriented along the x -axis. A modified one-dimensional hybrid code³⁰ is used to study the nonlinear dynamical evolution of the Alfvénic wave packets. In our simulations, electrons are treated as an isothermal fluid whereas the protons are treated as particles. For the high-resolution studies, we take the simulation box length as $860 V_A/\Omega_p$ (ion inertial lengths) with 2048 grid points and 200 particles in each cell. Simulations are carried out using periodic boundary conditions. For the initial condition, we take the exact solution^{8,13} of the DNLS equation, namely

$$B(x, t=0) = \frac{(2^{1/2}-1)^{1/2} B_s e^{i\theta(x)}}{[2^{1/2} \cosh(2V_s x) - 1]^{1/2}}, \quad (1)$$

where B_s is the amplitude of the soliton,

$$\theta(x) = -V_s x + \frac{3}{8(1-\beta)} \int_{-\infty}^{2x} |B|^2 dx', \quad (2)$$

and V_s is the soliton speed defined by

$$V_s = \frac{(2^{1/2}-1)B_s^2}{8(1-\beta)}. \quad (3)$$

Throughout, we use the normalized variables e.g., \mathbf{B} is normalized to B_0 , ρ to ρ_0 , \mathbf{v} to $V_A = B_0/(4\pi\rho_0)^{1/2}$ (V_A being the Alfvén velocity), t to the inverse of Ω_i , the ion cyclotron frequency and l to V_A/Ω_i , the ion inertial length. The subscript ‘0’ refers to the equilibrium quantities. Note that Eq. (1) is the left-hand polarized [$B = (B_y + iB_z)$] super-Alfvénic soliton solution, in the wave frame of reference,¹³ of the DNLS equation that is given by

$$\frac{\partial B_{\pm}}{\partial t} + \frac{1}{4(1-\beta)} \frac{\partial}{\partial x} (B_{\pm} |B_{\pm}|^2) \pm \frac{i}{2} \frac{\partial^2 B_{\pm}}{\partial x^2} = 0. \quad (4)$$

The plus and minus signs in the last term on the left-hand side of Eq. (4) correspond to left ($B_+ = B$) and right-hand (with $B_- = B_y - iB_z$) polarization, respectively.

In writing Eq. (1), we have taken the wave propagation along the direction of the ambient magnetic field and $\partial/\partial y = \partial/\partial z = 0$. Consistent with the DNLS solution given by Eq. (1), for the initial density and the velocity, we have used the relations

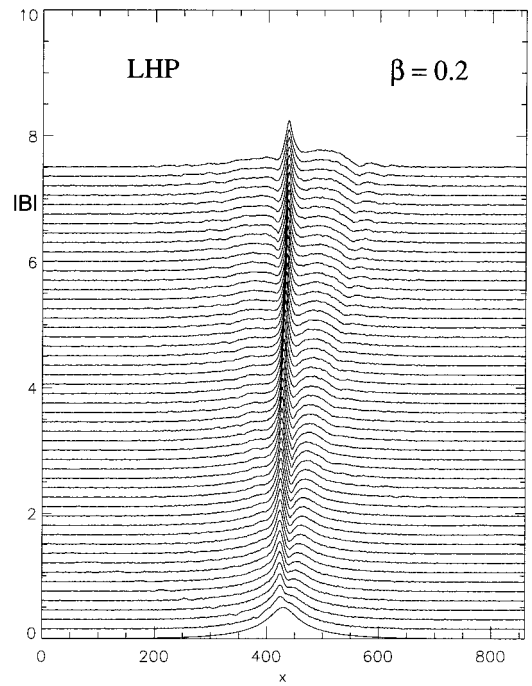


FIG. 1. Spatio-temporal evolution of $|B|$ for the left-hand polarized wave packet for $\beta=0.2$ and $B_s=0.5$.

$$\rho(x, t=0) = 1 + \frac{1}{2(1-\beta)} |B(x, t=0)|^2, \quad (5)$$

and $v_{y,z} = -B_{y,z}$. We may point out that the second term on the right-hand side of Eq. (5) is due to the density fluctuations driven by the pondermotive force generated by the magnetic field fluctuations. Even though the plasma, under consideration, is uniform with homogeneous magnetic field B_0 , effectively we are dealing with nonuniform plasma embedded in an inhomogeneous magnetic field because of the initial profiles used [cf. Eqs. (1) and (5)]. We will elaborate on this in the following sections. The code of Winske and Leroy³⁰ has been appropriately modified to include the localized inhomogeneities introduced by our specific initial conditions.

III. SIMULATION RESULTS

As mentioned in the Introduction, large-amplitude Alfvén waves have been observed in a variety of plasmas with very different plasma β . For example, in the solar wind β spans from <1 to >1 . So to model the nonlinear dynamical behavior of these waves in a variety of such systems, we have used β as a parameter. All the results reported in this paper are in the wave packet frame of reference. The spatio-temporal evolution of the wave packet for $\beta=0.2$ is shown in a stack plot in Fig. 1. To avoid overlapping of the packets at different times, we have advanced $|B|$ by 0.15 at each time step which corresponds to 20 gyroperiods. The time span for the simulations reported here is 1000 gyroperiods. From Fig. 1, one clearly sees the wave packet collapsing. Evolution for $\beta=0.6$ is shown in Fig. 2. For larger β (>0.2) (results for $\beta=0.3$ and 0.4 not shown here) the collapse stops at a critical time t_c which is a function of β and B_s (cf. Fig. 4), the

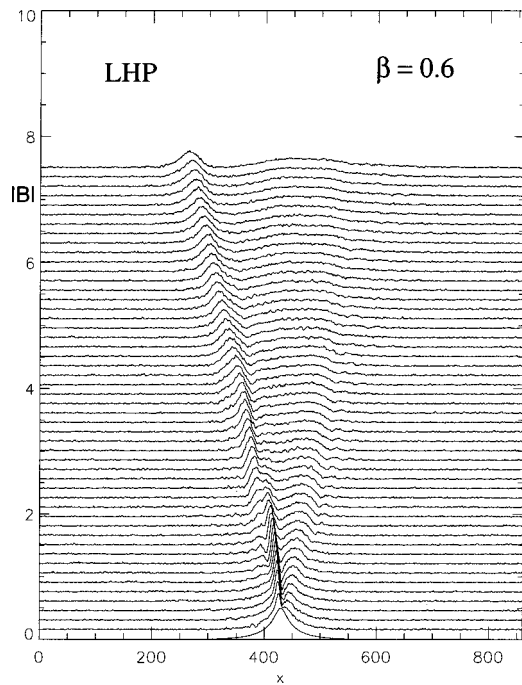


FIG. 2. Spatio-temporal evolution of $|B|$ for the left-hand polarized wave packet for $\beta=0.6$ and $B_s=0.5$.

initial amplitude of the packet. This happens at a dynamical turning point which is characterized by $\partial\omega(k)/\partial k=0$. At this point polarization changes from LHP to RHP and the wave packet starts dispersing and broadening. One can roughly understand this behavior from the nonlinear dispersion relation corresponding to Eq. (4); this in the wave frame of reference is given by

$$\omega \approx k|B(x,t)|^2/(1-\beta) \pm \mu k^2, \quad (6)$$

where μ is some constant and ω and k are the wave frequency and the wave number. In Eq. (6), for wave propagation along the positive x direction and for $\beta < 1$, plus and minus signs correspond to the RHP and the LHP, respectively. On the right-hand side of Eq. (6), first term is due to the nonlinear term of the DNLS and the second term is due to the dispersive contribution of the DNLS. We may point out that Eq. (6) with B replaced by B_s represents the criterion for the modulational instability for the linearized DNLS equation. As time progresses, both $|B|$ as well as k change; Eq. (6) reflects the corresponding changes in the frequency ω . For the case of LHP, these two contributions due to nonlinearity and due to dispersion compete with each other and because of this competition, the packet starts shrinking, i.e., k starts increasing. The moment the second term exceeds the first term; the real part of ω becomes negative. At this juncture, one encounters the turning point since the group velocity of the packet, i.e., $\partial\omega(k)/\partial k$ changes sign. As a result, ω starts increasing with an increase in k and hence the wave packet starts dispersing and broadening. This leads to a reversal of polarization from LHP to RHP. A word of caution may be in order here. The reversal at the dynamical turning point (characterized by the critical time t_c), in our simulations, is not equivalent to the simple reflection of the wave

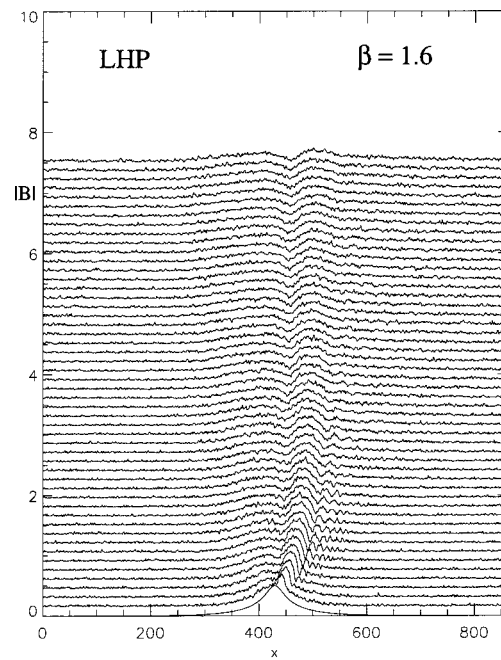


FIG. 3. Spatio-temporal evolution of $|B|$ for the left-hand polarized wave packet for $\beta=1.6$ and $B_s=0.5$.

packet since after reversal it has different polarization properties. We would like to emphasize that Eq. (6) is not an exact nonlinear relation since it corresponds to the evolution equation that neglects fifth and higher order nonlinearities. It may be worth pointing out that the collapse of electrostatic wave packets governed by the Nonlinear Schrödinger equation^{31,32} occurs only in systems with more than one spatial dimension. In our case, however, the collapse of Alfvén wave packets is due to the dynamical evolution and is found even in one-dimensional systems.

From Figs. 1 and 2, we see that t_c decreases with an increase in β . From our simulations for $\beta=0.3$ and 0.4 (not shown here), we find that $t_c(\beta=0.3) > t_c(\beta=0.4) > t_c(\beta=0.6)$. According to Eq. (2), in a system with $\beta > 1$, the LHP wave packet would behave like an RHP wave packet and vice-versa. Consequently for $\beta=1.6$ in Fig. 3, we do not see any collapse associated with the LHP packet. It indeed behaves like a RHP packet that moves to the right, i.e., it is accelerated and at the same time it emits high-frequency radiations. The result of increasing the initial amplitude of the wave packet to $B_s=0.7$ instead of $B_s=0.5$ used for Figs. 1–3, is shown in Fig. 4. In this case we see a rather different evolution for $\beta=0.2$. On comparing Fig. 1 with Fig. 4, we find that the turning point occurs much earlier for wave packets with larger initial amplitudes. The decrease of t_c with an increase in β and in B_s is as one would have expected because of the following reasons. The local inhomogeneities introduced by the density fluctuations driven by the ponderomotive force generated by the large-amplitude Alfvén waves, according to Eq. (5), are stronger for larger β (for $\beta < 1$) as well as for a larger initial amplitude of the wave packet, i.e., $B_s \equiv B(x, t=0)$. Consequently the coupling between the density fluctuations and the magnetic field fluctuations becomes stronger when β and/or B_s is increased. The

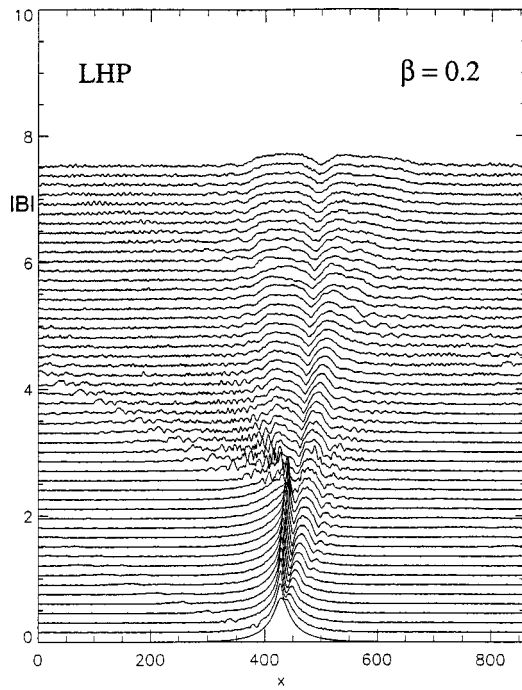


FIG. 4. Spatio-temporal evolution of $|B|$ for the left-hand polarized wave packet for $\beta=0.2$ but with $B_s=0.7$.

collapsing of Alfvénic wave packets reported in the present paper is an outcome of this coupling. Because of stronger coupling, k increases at a faster rate; this in turn reduces t_c . The phenomena of collapse, that we are observing, could be considered as a process for transporting energy to larger wave numbers. Since t_c decreases with an increase in β , we may conclude that the rate of transport of energy is faster in case of plasmas with larger β .

The temporal evolution of the amplitude B_{\max} (\equiv to the maximum value of $|B|$) of the initial LHP wave packet with β is shown in Fig. 5. The initial amplitude for all these cases is 0.5. Note that $B_{\max}(t=0) \equiv B_s$. It is interesting to note that the amplitude first starts increasing but after the turning point, it starts decreasing. For example, for $\beta=0.4$, this changeover takes place at $t \sim 380$ compared to $t_c \sim 550$ for $\beta=0.3$. This clearly shows that for larger β ($\beta < 1$), kinetic effects come into the picture relatively earlier. One can explain this behavior as follows. The width of the wave packet

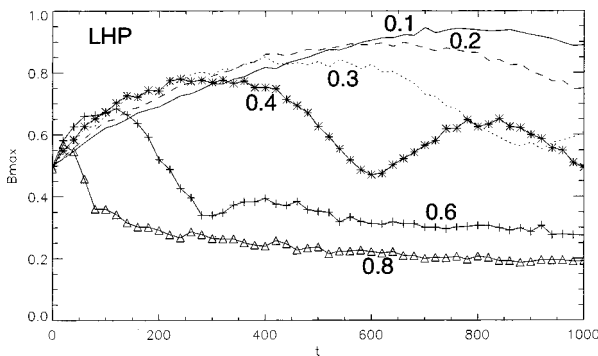


FIG. 5. Temporal evolution of the amplitude of the initial left-hand polarized wave packet for $\beta=0.1, 0.2, 0.3, 0.4, 0.6,$ and 0.8 .

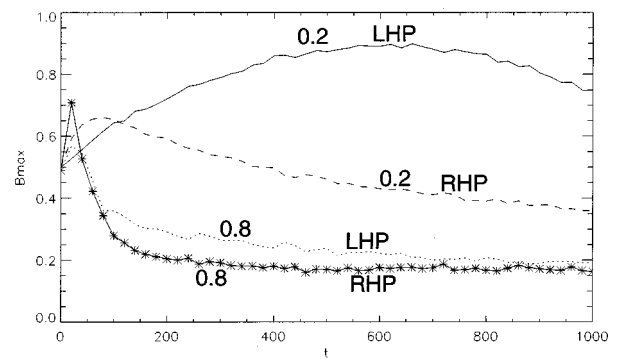


FIG. 6. Temporal evolution of the amplitude of the initial left-hand (LHP) and right-hand (RHP) polarized wave packets for $\beta=0.2$ and 0.8 .

as given by Eq. (1) is inversely proportional to V_s which is given by Eq. (3). Correspondingly the scale sizes of the wave packets are smaller for larger B_s and larger β (for $\beta < 1$). As a consequence, kinetic effects become rather significant within shorter intervals of time compared to the ones corresponding to lower values of β and B_s .

As mentioned earlier, the LHP mode, at the turning point, turns into the RHP mode. This is further confirmed by comparing the amplitude variations with time for LHP and RHP shown in Fig. 6. Variation of the amplitude with B_s , for a given β , is shown in Fig. 7. This shows the sensitive dependence of the turning point on the initial amplitude.

We also looked into the spatio-temporal evolution of the density fluctuations N . They seem to be driven by the magnetic field fluctuations. It is interesting to observe that the stack plots, for different β , for N overlap the ones for $|B|$ (cf. Figs. 8 and 9). From these results, we conclude that the ponderomotive force is the dominant force in the evolution of the ion density. One would expect similar behavior for the density fluctuations from the DNLS equation also. In these simulations, we do not observe ion-acoustic waves; their absence could be attributed to the electron (T_e) and the ion temperature (T_i) being equal for all the cases discussed here. For plasmas with $\beta \sim 1$ and $T_e \gg T_i$, we do observe ion-acoustic waves and the associated Landau damping for cases with $T_e \lesssim T_i$.

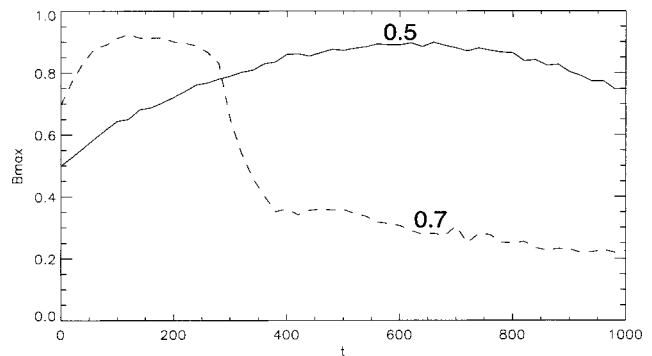


FIG. 7. Temporal evolution of the amplitude of the initial left-hand (LHP) polarized wave packets for $\beta=0.2$ and $B_s=0.5$ and 0.7 .

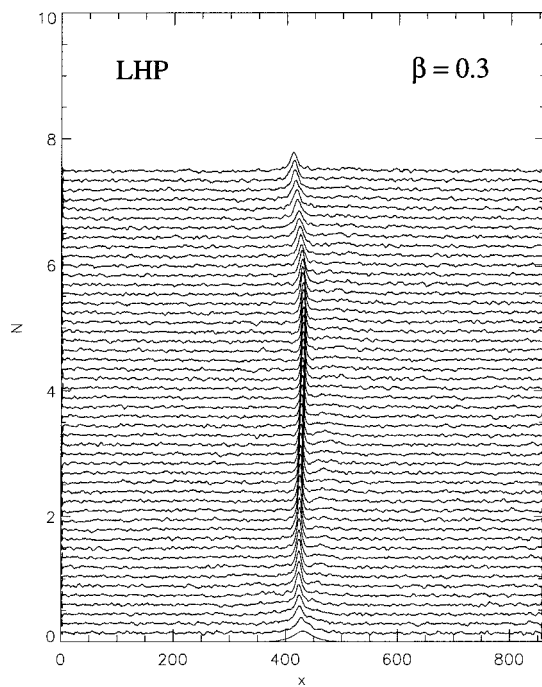


FIG. 8. Spatio-temporal evolution of the density fluctuations N for the left-hand polarized wave packet for $\beta=0.3$ and $B_s=0.5$.

IV. DISCUSSION AND CONCLUSIONS

We have investigated the nonlinear spatio-temporal evolution of the Alfvénic wave packets by means of high resolution hybrid simulations. Unlike the evolution governed by the DNLS equation, in our simulations we can consider large-amplitude waves and also span the entire plasma β range including β in the neighborhood of unity. Moreover, both the compressive, as well as the dispersive, effects are

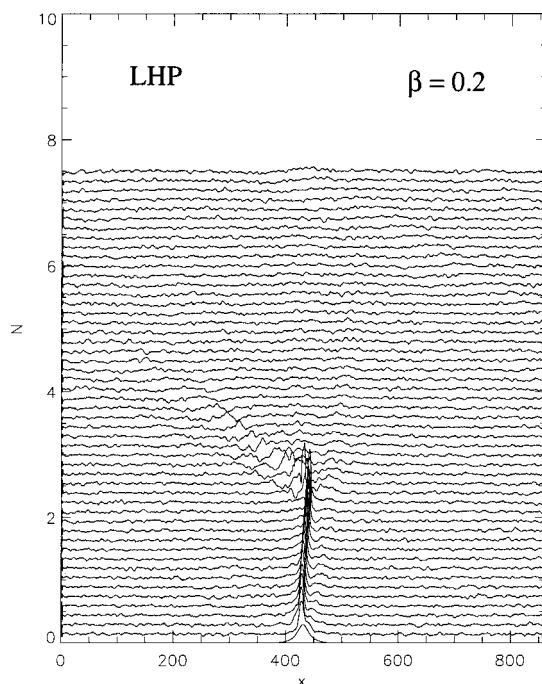


FIG. 9. Spatio-temporal evolution of the density fluctuations N for the left-hand polarized wave packet for $\beta=0.2$ and $B_s=0.7$.

properly accounted for. Polarization of the large-amplitude Alfvén waves is known to play a very crucial role in determining their stability characteristics. For example, for $\beta < 1$, LHP waves are modulationally unstable but the RHP waves are stable and vice-versa for systems with $\beta > 1$. Our simulations not only confirm this but also exhibit an interesting phenomena of collapse of the LHP wave packets. When the size of the wave packet becomes sufficiently small (\sim a few Larmor radii/ ion inertial lengths), the kinetic effects become significant. The latter, in fact, in our case arrest the blowing up of the wave packets that we encounter in our dispersive MHD simulations. In our earlier studies,¹⁹ of the evolution of these wave packets by means of Hall MHD simulations, we did not observe any collapsing LHP wave packets. We had missed these interesting features, since we had not done very high-resolution investigations.

In the present paper, we show that the Alfvénic system behaves like a *Nonlinear Dynamical* system. Associated with the phenomena of collapse, we observe the dynamical turning point. At this turning point, the polarization of the wave packet flips from LHP to RHP. From our simulations, we find that the turning point crucially depends on the plasma β as well as the initial amplitude of the wave packet. We also observe that the density fluctuations are very well correlated with the magnetic field fluctuations. Physically collapse means the transport of energy to larger k values, i.e., the cascading process. In order to look for the potential applications of these collapsing Alfvénic wave packets, we repeated our simulations (not presented here) for initial density profiles different than the one given by Eq. (5). One of the cases we considered is with zero density fluctuations, i.e., $\rho(x, t=0) = 1$. In all these cases, we observe the collapse of LHP wave packets; some small quantitative differences are found but no qualitative changes whatsoever. During the evolution of the wave packet, density fluctuations are generated by the ponderomotive force of the large magnetic field fluctuations.

In summary, our simulations confirm that the source of collapse is the coupling between magnetic field fluctuations and density fluctuations. The scale sizes of the wave packets decrease at a faster rate for larger initial amplitudes and for plasmas with larger β . As mentioned earlier, collapse can provide an efficient channel for transport of energy; one could look for its potential applications in space plasmas with large β .

ACKNOWLEDGMENTS

The research conducted at the Jet Propulsion Laboratory, California Institute of Technology, was performed under contract to the National Aeronautics and Space Administration. B.B. would like to thank the National Research Council for the financial support and would also like to acknowledge some fruitful discussions with E. Smith and B. T. Tsurutani.

¹M. Pettini, L. Nocera, and A. Vulpiani, in *Chaos in Astrophysics*, edited by J. R. Buchler *et al.* (Reidel, Dordrecht, 1985), p. 305.

²G. S. Lakhina and B. Buti, *Sol. Phys.* **99**, 277 (1985); *Astrophys. J.* **327**, 1020 (1988); **352**, 747 (1990).

³S. R. Spangler, *Astrophys. J.* **376**, 540 (1991).

⁴V. Jatenco-Pereira, *Phys. Scr.* **T60**, 113 (1995).

- ⁵J. W. Belcher and L. Davis, *J. Geophys. Res.* **76**, 3534 (1971).
- ⁶F. L. Scarf, F. V. Coroniti, C. F. Kennel *et al.*, *Science* **232**, 377 (1986).
- ⁷B. T. Tsurutani, E. J. Smith, H. Matsumoto *et al.*, *Geophys. Res. Lett.* **17**, 757 (1990).
- ⁸D. J. Kaup and A. C. Newell, *J. Math. Phys.* **19**, 798 (1978).
- ⁹C. F. Kennel, B. Buti, T. Hada, and R. Pellat, *Phys. Fluids* **31**, 1949 (1988).
- ¹⁰B. Buti, "Nonlinear and chaotic Alfvén waves," in *Solar and Planetary Plasma Physics*, edited by B. Buti (World Scientific, Singapore, 1990), p. 92.
- ¹¹A. Rogister, *Phys. Fluids* **14**, 2733 (1971).
- ¹²T. Hada, C. F. Kennel, and B. Buti, *J. Geophys. Res.* **94**, 65 (1989).
- ¹³F. Verheest and B. Buti, *J. Plasma Phys.* **47**, 15 (1992).
- ¹⁴E. Mjølhus and J. Wyller, *Phys. Scr.* **33**, 442 (1986); *J. Plasma Phys.* **40**, 299 (1988).
- ¹⁵S. R. Spangler, *Phys. Fluids B* **1**, 1738 (1989); **2**, 407 (1990).
- ¹⁶M. V. Medvedev and P. H. Diamond, *Phys. Plasmas* **3**, 863 (1996).
- ¹⁷T. Hada, *Geophys. Res. Lett.* **20**, 2415 (1993).
- ¹⁸A. Roychoudhury, B. Buti, and B. Dasgupta, *Aust. J. Phys.* **51**, 125 (1997).
- ¹⁹B. Buti, V. Jayanti, A. F. Viñas, S. Ghosh, M. L. Goldstein, D. A. Roberts, G. S. Lakhina, and B. T. Tsurutani, *Geophys. Res. Lett.* **25**, 2377 (1998).
- ²⁰M. Velli, B. Buti, B. E. Goldstein, and R. Grappin, "Propagation and disruption of Alfvénic solitons in the expanding solar wind," in *Solar Wind Nine*, AIP Proceedings 471, edited by S. Habbal *et al.* (American Institute of Physics, Woodbury, NY, 1999), p. 445.
- ²¹S. Ghosh and K. Papadopoulos, *Phys. Fluids* **30**, 1371 (1987).
- ²²T. Hada, C. F. Kennel, B. Buti, and E. Mjølhus, *Phys. Fluids B* **2**, 2581 (1990).
- ²³N. Nocera and B. Buti, "Low dimensional structures in numerical simulations of DNLS," *Proceedings of the 94 International Congress on Plasma Physics*, edited by P. H. Sakanaka, E. Del Bosco, and N. V. Alves (American Institute of Physics, Melville, NY, 1995), p. 115.
- ²⁴N. Nocera and B. Buti, *Phys. Scr.* **T63**, 186 (1996).
- ²⁵N. Nocera and B. Buti, "Bifurcations of coherent states of the DNLS equation," in *New Perspectives in the Physics of Mesoscopic Systems*, edited by S. De Martino *et al.* (World Scientific, Singapore, 1997), p. 225.
- ²⁶N. Nocera and B. Buti, *Plasma Phys. Controlled Fusion* **22**, 2295 (1998).
- ²⁷B. Buti and L. Nocera, "Chaotic Alfvén waves in the solar wind," in *Ref.* **20**, p. 173.
- ²⁸B. Buti, *Nonlinear Process. Geophys.* **6**, 129 (1999).
- ²⁹B. Buti, V. L. Galinski, V. I. Shevchenko, G. S. Lakhina, B. T. Tsurutani, B. E. Goldstein, P. Diamond, and M. V. Medvedev, *Astrophys. J.* **523**, 849 (1999).
- ³⁰D. Winske and M. M. Leroy, "Hybrid simulation techniques applied to the Earth's bow shock," in *Computer Simulations of Space Plasmas*, edited by H. Matsumoto and T. Sato (Reidel, Hingham, MA, 1985), p. 25.
- ³¹B. Buti, *Phys. Rev. Lett.* **38**, 498 (1977).
- ³²V. E. Zakharov, "Collapse and self-focusing of Langmuir waves," in *Handbook of Plasma Physics*, edited by M. N. Rosenbluth and R. Z. Sagdeev (Elsevier, New York, 1984), p. 81.